CHEMISTRY OF MATERIALS
Article

Chem. Mater. **2010,** *22,* 6555–6563 6555
DOI:10.1021/cm102030p

Highly Size-Controlled, Low-Size-Dispersity Nickel Nanoparticles from Poly(propylene imine) Dendrimer−Ni(II) Complexes

Elisabeta Mitran, Barry Dellinger, and Robin L. McCarley*

Department of Chemistry, Louisiana State University, Baton Rouge, Louisiana 70803-1804, United States

Received July 21, 2010. Revised Manuscript Received November 11, 2010

Reported here is the highly controlled synthesis and subsequent characterization of low-size-dispersity (±8−21%) crystalline Ni(0) nanoparticles derived from a dendrimer-ligand-based method employing amine-terminated poly(propylene imine) dendrimers, DAB-Am$_n$. Crystalline Ni(0) nanoparticles devoid of any nickel boride are obtained by anaerobic borohydride reduction in methanol of DAB-Am$_n$−Ni(II)$_x$, as determined by high-resolution X-ray photoelectron spectroscopy (XPS), high-resolution transmission electron microscopy (HR-TEM), and selected-area electron diffraction (SAED) measurements. Nickel nanoparticles with highly tunable diameters ranging from 1.9 to 2.7 nm are readily obtained by methanolic borohydride reduction of Ni(II) coordinated to the primary amines of five different generations of DAB-Am$_n$ (n = 4, 8, 16, 32, 64). Control over the diameter of the Ni nanoparticles is readily achievable and inversely related to dendrimer generation and the NH_2:Ni(II) ratio, n/x. These outcomes bode well for future studies of relationships between metal nanoparticle properties and their behavior in the catalytic production of pollutants that have been found in combustion sources.

1. Introduction

Particles produced in combustion chambers in the gas phase undergo inception, coagulation, and surface growth, and as a result, their size ranges from 2−4 nm for the smallest metallic nanoparticles, to a few hundred nanometers for agglomerates.[1] Under primarily oxidative/oxidative pyrolysis of fuels, metal nuclei or supported metal nanoparticles may form and result in initiation of pollutant production on their surfaces.[2] Several different transition metals are present in various fuels, including Cu, Fe, V, and Ni,[1] and it is expected that the type and quantity of a given pollutant produced during the combustion process will be a function of metal identity and size. For example, Van den Brink et al.[3] showed that in comparison to larger-sized Pt particles, supported Pt nanoparticles with very small size were more active in formation of polychlorinated benzene in the catalytic combustion of chlorobenzene. We propose that similar effects with Ni nanoparticles will occur, and there may exist relationships between particle size and both the nature and amount of pollutant products formed during particle-catalyzed reactions. However, what is needed is a simple route to the routine formation of zerovalent Ni nanoparticles in the 1−3 nm diameter range with tunable size control.

The synthesis of metallic nickel nanoparticles is challenging because of their reactivity and the limitations of existing synthetic routes. Gas-phase routes include hydrogen reduction of $NiCl_2$,[4] hydrogen plasma metal reaction,[5] and DC sputtering in argon,[6] with the smallest nanoparticles having diameters $d \geq 31$ nm. Liquid-phase methods—such as microemulsion/surfactant techniques,[7−10] chemical reduction in solution[11−16] or in the presence of heterogeneous

*Corresponding author. Phone: (225) 578−3239. Fax: (225) 578−3458. E-mail: tunnel@LSU.edu.

(1) Allouis, C.; Beretta, F.; D'Alessio, A. *Chemosphere* **2003**, *51*, 1091–1096.
(2) Walsh, M.; Cormier, S.; Varner, K.; Dellinger, B. EM Mag. **2010**, April, 26−30.
(3) van den Brink, R. W.; Krzan, M.; Feijen-Jeurissen, M. M. R.; Louw, R.; Mulder, P. *Appl. Catal., B* **2000**, *24*, 255–264.
(4) Suh, Y. J.; Jang, H. D.; Chang, H. K.; Hwang, D. W.; Kim, H. C. *Mater. Res. Bull.* **2005**, *40*, 2100–2109.
(5) Duan, H.; Lin, X.; Liu, G.; Xu, L.; Li, F. *J. Mater. Process. Technol.* **2008**, *208*, 494–498.
(6) Rellinghaus, B.; Stappert, S.; Wassermann, E. F.; Sauer, H.; Spliethoff, B. *Eur. Phys .J. D* **2001**, *16*, 249–252.
(7) Wu, S. H.; Chen, D. H. *J. Colloid Interface Sci.* **2003**, *259*, 282–286.
(8) Chen, D. H.; Wu, S. H. *Chem. Mater.* **2000**, *12*, 1354–1360.
(9) Legrand, J.; Taleb, A.; Gota, S.; Guittet, M. J.; Petit, C. *Langmuir* **2002**, *18*, 4131–4137.
(10) Chiang, S.-J.; Liaw, B.-J.; Chen, Y.-Z. *Appl. Catal., A* **2007**, *319*, 144–152.
(11) Hou, Y.; Kondoh, H.; Ohta, T.; Gao, S. *Appl. Surf. Sci.* **2005**, *241*, 218–222.
(12) Chen, L.; Chen, J. M.; Zhou, H. D.; Zhang, D. J.; Wan, H. Q. *Mater. Sci. Eng., A* **2007**, *452*, 262–266.
(13) Couto, G. G.; Klein, J. J.; Schreiner, W. H.; Mosca, D. H.; de Oliveira, A. J. A.; Zarbin, A. J. G. *J. Colloid Interface Sci.* **2007**, *311*, 461–468.
(14) Roy, A.; Srinivas, V.; Ram, S.; De Toro, J. A.; Goff, J. P. *J. Appl. Phys.* **2006**, *100*, 094307.
(15) Sidhaye, D. S.; Bala, T.; Srinath, S.; Srikanth, H.; Poddar, P.; Sastry, M.; Prasad, B. L. V. *J. Phys. Chem. C* **2009**, *113*, 3426–3429.
(16) Kudlash, A. N.; Vorobyova, S. A.; Lesnikovich, A. I. *J. Phys. Chem. Solids* **2008**, *69*, 1652–1656.
(17) Boudjahem, A. G.; Monteverdi, S.; Mercy, M.; Bettahar, M. M. *Langmuir* **2004**, *20*, 208–213.
(18) Estournes, C.; Lutz, T.; Happich, J.; Quaranta, T.; Wissler, P.; Guille, J. L. *J. Magn. Magn. Mater.* **1997**, *173*, 83–92.
(19) Chatterjee, A.; Chakravorty, D. *Appl. Phys. Lett.* **1992**, *60*, 138–140.

Published on Web 12/07/2010

supports,[17,18] and organometallic routes,[19] including thermolytic decomposition[20−22]—typically result in nanoparticles with $d \geq 3$ nm, and with size control only for particles above 5 nm.[20,22,23] At present, we are unaware of a simple solution method, without using unimolecular templates such as dendrimers,[24−30] that allows for careful control of Ni particle size over a range of sizes with $d < 3$ nm and with low size dispersity. Also, formation of Ni(0) particles free of boride contaminants, when using borohydride reducing agents in a variety of solvents, is a significant issue.[9]

To address these challenges, we turned to a nascent alternative methodology having the potential to form Ni nanoparticles with $d < 3$ nm, namely that which employs dendrimers.[24] In an initial report, Knecht et al. prepared two sizes of ferromagnetic nickel nanoparticles with diameters of 0.8 ± 0.2 and 1.2 ± 0.3 nm by sodium triethylborohydride reduction of a 50% dodecyl-functionalized, sixth-generation PAMAM dendrimer coordinated to Ni(II) with toluene as solvent.[24] We describe here a chemically distinct and simple synthetic route that leads to zerovalent, contaminant-free crystalline nickel nanoparticles, $Ni(0)_{NP}$, whose diameters can be systematically tuned from 1.9 to 2.7 nm with a very low size dispersity. These unprecedented results for the formation of Ni(0) nanoparticles are achieved by use of a readily available, simple, and powerful hydride-ester-based reducing agent[31] and unmodified, commercially available poly(propylene imine) dendrimers of five different generations. Specifically, this is accomplished by anerobic, methanolic borohydride reduction of stoichiometrically well-defined Ni(II)-dendrimer complexes that are based on coordination of Ni(II) to the dipropyltriamine groups at the periphery of the poly(propylene imine) dendrimers. By systematic control of the Ni(II)-dipropyltriamine ratio for a given dendrimer generation, as a function of the five different dendrimer generations, we are able to prepare highly tunable, statistically different-sized Ni nanoparticles with low size dispersity ($< \sim 20\%$). Furthermore, with high signal-to-noise ratio X-ray photoelectron spectroscopy experiments, we unequivocally demonstrate that the Ni nanoparticles are in the zerovalent state, and we also show that the $Ni(0)_{NP}$ materials do not contain nickel borides—a very common challenge in the chemical reduction of Ni(II) with sodium borohydride[9]—as noted by outcomes from high-resolution transmission electron microscopy, selected-area electron diffraction, and X-ray photoelectron spectroscopy experiments.

2. Experimental Section

Materials. Commercial-grade reagents were used without further purification. The poly(propylene imine) dendrimers were obtained from Sigma-Aldrich (generations 1 and 3) and SYMO-Chem (generations 2, 4, and 5) and used as received. $NiCl_2 \cdot 6H_2O$ (99.9%), Ni_2B (30 mesh, 99%), Ni nanopowder (≤100 nm particle size, 99.9% trace metal basis), and $NaBH_4$ were purchased from Sigma-Aldrich. HPLC-grade methanol was from EMD.

UV−Visible Spectroscopy. The measurements were performed in a quartz cell (1 cm optical path length), and spectra were recorded after stirring, using a CARY 50 BIO UV/visible spectrophotometer. Stock solutions of 5, 10×10^{-3}, and 20×10^{-3} M DAB-Am_n dendrimers (with respect to primary amine end group) and 5 and 10×10^{-3} M Ni(II) salt solutions were prepared in methanol to investigate the stoichiometry of the predominant complex. The method of continuous variation (Job plot) was used to determine the stoichiometry.[32,33] Solutions were prepared (to obtain a total volume of 2 mL) by mixing aliquots of equimolar solutions of Ni(II) salt and DAB-Am_n dendrimer such that the combined molar concentration of Ni(II) plus dendrimer was constant (1×10^{-2} M) but the relative mole fractions of Ni(II) and -NH_2 end groups were varied in a compensatory manner. The absorbance of each solution was measured at two wavelengths (640 and 680 nm) and plotted, after correction, versus mole fraction of NH_2 (mole NH_2/(mole NH_2 + mole Ni(II))). All Ni(II) absorbance spectra for Job plots were background corrected. Complexation of Ni(II) with DAB-Am_n dendrimer was determined by spectrophotometric titrations in which aliquots of 50−100 μL of DAB-Am_n dendrimer solution (20×10^{-3} M) were added to Ni(II) solution (5×10^{-3} M) of a known volume. The titrations were made in a quartz cell (1 cm optical path length) and spectra were recorded after stirring. The titration end point was determined by extrapolating the two linear regions. All spectra were corrected for dilutions.

Preparation of DAB-Am_n−$Ni(II)_x$ Complexes and DAB-Am_n−$Ni(0)_{NP}$ Nanoparticles. The nomenclature used to describe the dendrimers and dendrimer-nanoparticles in this paper is as follows: poly(propylene imine) dendrimer is DAB-Am_n, where n is the number of primary NH_2 (Am) end groups; complexes of poly(propylene imine) dendrimer with Ni(II) are referred to as DAB-Am_n−$Ni(II)_x$, where x is $n/4$, $n/2$, or $n/8$; and the poly(propylene imine) dendrimer loaded with metal ions after reduction is referred to as DAB-Am_n−$Ni(0)_{NP}$.

The dendrimer−nickel complexes were synthesized in the following mode: the requisite amounts of methanolic solutions of Ni(II) and the corresponding amine-terminated poly(propylene imine) dendrimer were mixed to result in a final Ni(II) concentration of 5×10^{-4} M for the different stoichiometric ratios studied. Investigations of nanoparticle size as a function of nickel chloride concentration (5×10^{-4} M and 2×10^{-3} M) and the NH_2:Ni(II) ratio (n/x) in the dendrimer precursor were also carried out. DAB-Am_n−$Ni(0)_{NP}$ were obtained by chemical reduction of DAB-Am_n−$Ni(II)_x$ solutions

(20) Johnston-Peck, A. C.; Wang, J.; Tracy, J. B. *ACS Nano* **2009**, *3*, 1077–1084.
(21) Park, J.; Kang, E.; Son, S. U.; Park, H. M.; Lee, M. K.; Kim, J.; Kim, K. W.; Noh, H. J.; Park, J. H.; Bae, C. J.; Park, J. G.; Hyeon, T. *Adv. Mater.* **2005**, *17*, 429–434.
(22) Wang, H.; Jiao, X.; Chen, D. *J. Phys. Chem. C* **2008**, *112*, 18793–18797.
(23) Winnischofer, H.; Rocha, T. C. R.; Nunes, W. C.; Socolovsky, L. M.; Knobel, M.; Zanchet, D. *Acs Nano* **2008**, *2*, 1313–1319.
(24) Knecht, M. R.; Garcia-Martinez, J. C.; Crooks, R. M. *Chem. Mater.* **2006**, *18*, 5039–5044.
(25) Floriano, P. N.; Noble, C. O.; Schoonmaker, J. M.; Poliakoff, E. D.; McCarley, R. L. *J. Am. Chem. Soc.* **2001**, *123*, 10545–10553.
(26) Chai, M.; Holly, A. K.; Norton, M. L. *Polym. Prepr.* (*Am. Chem. Soc., Div. Polym. Chem.*) **2003**, *44*, 296–297.
(27) Sun, X.; Dong, S.; Wang, E. *Macromolecules* **2004**, *37*, 7105–7108.
(28) Esumi, K.; Isono, R.; Yoshimura, T. *Langmuir* **2004**, *20*, 237–243.
(29) Vohs, J. K.; Brege, J. J.; Raymond, J. E.; Brown, A. E.; Williams, G. L.; Fahlman, B. D. *J. Am. Chem. Soc.* **2004**, *126*, 9936–9937.
(30) Auten, B. J.; Hahn, B. P.; Vijayaraghavan, G.; Stevenson, K. J.; Chandler, B. D. *J. Phys. Chem. C* **2008**, *112*, 5365–5372.
(31) Kim, J.; De Castro, K. A.; Lim, M.; Rhee, H. *Tetrahedron* **2010**, *66*, 3995–4001.
(32) Job, P. *Ann. Chim. Fr.* **1928**, *9*, 113–203.
(33) Huang, C. Y. *Methods Enzymol.* **1982**, *87*, 509–525.

with a 10-fold molar excess of methanolic $NaBH_4$ solution under nitrogen in a glovebag. Immediately upon its preparation (3−5 min), the methanolic $NaBH_4$ solution (0.5 mL) was added to the DAB-Am_n−Ni(II)$_x$ solutions drop by drop over a 30 s interval. The reduction resulted in an instantaneous color change of the solution from pale green to black, indicating the formation of nanoclusters of DAB-Am_n-Ni(0)$_{NP}$. The nickel nanoparticle solutions are very sensitive to atmospheric air; after exposure to air for times greater than 10 min, the solutions become colorless. If the nanoparticles are kept under nitrogen atmosphere, no change in color is observed for up to the longest time investigated, 2 weeks. The metal nanoparticles obtained were analyzed by UV−visible absorption spectroscopy, X-ray photoelectron spectroscopy (XPS), and high-resolution transmission electron microscopy (HR-TEM).

TEM Images of DAB-Am_n−Ni(0)$_{NP}$. Electron microscopy images were obtained with a JEM-2010 high-resolution transmission electron microscope. A drop of the analyte solution was placed on a Formvar carbon-coated copper grid under an inert atmosphere in a glovebag, and the solvent was allowed to evaporate. The sample was exposed to air briefly (less than 60 s) during transfer from the glovebag to the microscope. The JEM-2010 was operated at an accelerating voltage of 200KV and different standard magnifications (400 and 600K). For each sample, at least 270 particles from different parts of the grid were used to determine the average diameter and size distribution of particles.

X-ray Photoelectron Spectroscopy (XPS). The XPS data were obtained with an AXIS 165 photoelectron spectrometer using a monochromatized Al Kα X-ray radiation source. First, the metal nanoparticles were adsorbed onto clean Pt foil substrates under anaerobic conditions for at least 48 h. The Pt foil was removed from solution and dried with a stream of Ar in a glovebag before loading in the instrument. Samples were stored under Ar in the antechamber overnight and then moved into the analysis chamber for XPS study. A charge neutralizer was used to eliminate the charge effect on the sample surface. Low-resolution survey spectra (40 eV pass energy) were recorded for the 0−1200 eV region to determine the elements present in the sample. High-resolution spectra (160 eV pass energy) were recorded for the Ni 2p and B 1s regions. The binding energies were calibrated with respect to the signal of C1s (binding energy 284 eV). Before measurements, the samples were sputtered with Ar ions for 1 min (DAB-Am_n−Ni(0)$_{NP}$) or 10 min (for the reference standards) to avoid surface oxidation due to manipulation of samples in air during loading into the antechamber. For the XPS analyses, samples of the DAB-Am_n−Ni(0)$_{NP}$ produced from DAB-Am_n−Ni(II)$_x$ with a Ni(II) concentration of 5×10^{-3} M were used; the use of lower Ni(II) concentrations leads to low signal-to-noise ratio spectra.

3. Results and Discussion

Dendrimer-Nickel Complexes: DAB-Am_n−Ni(II)$_x$. Different generations of DAB-Am_n dendrimers were examined as possible multifunctional ligands for Ni(II) in methanol solutions. In the absence of dendrimer, Ni(II) exhibits a maximum absorption near $\lambda = 410$ nm and another absorption band that spans 680 to 790 nm (corresponding to d−d transitions[34]), Figure 1. The addition of the three

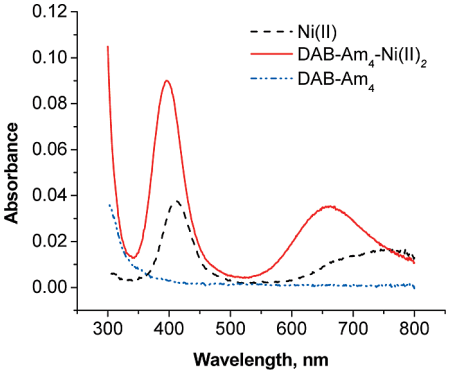

Figure 1. UV−visible absorption spectra of 5×10^{-3} M $NiCl_2 \cdot 6H_2O$ in methanol (dashed black line), 5×10^{-3} M $NiCl_2 \cdot 6H_2O$ with DAB-Am_4 fully complexed (solid red line), and DAB-Am_4 dendrimer (2×10^{-2} M in end groups, dotted/dashed blue line).

different generations of DAB-Am_n to Ni(II) solutions produced a light green color and is the result of Ni-NH_2 complexation. In the presence of DAB-Am_n, the absorption maximum of the d−d transition is shifted to 640 nm, and the band at 410 nm is now centered at 400 nm. The band intensities do not change for times up to 50 days (the longest time investigated), indicating that the initially formed complex is stable. As expected, the DAB-Am_n dendrimer does not absorb light to any significant degree in this energy range.

The method of continuous variation (Job plot) was used to identify the stoichiometry of the predominant Ni(II)-dendrimer complex as a function of dendrimer generation. This was achieved by mixing aliquots of equimolar solutions of Ni(II) and dendrimer such that the total concentration of Ni(II) plus dendrimer remained constant. To ensure proper identification of the stoichiometry of the Ni-dendrimer complex, measurements were taken at two wavelengths (640 and 680 nm) using total concentrations of Ni(II) plus dendrimer of 1×10^{-2} M. In Figure 2 are displayed Job plots for generations 1, 3, and 4 of DAB-Am_n dendrimers in the presence of various amounts of Ni(II) in methanol. It was observed for all generations investigated that the maximum value in the Job plots occurs at a NH_2:Ni(II) mole ratio of 2:1, a value that is in accord with results from spectrophotometric titrations we carried out (Figure 3) and those of others.[35,36] In prior spectrophotometric titration studies, it was demonstrated that Ni(II) does not complex with the tertiary amine functional groups in the core of DAB-Am_n dendrimers.[26,35,36] In those studies, it was shown that the predominant DAB-Am_4−Ni(II) complex has a 2:1 ratio of NH_2:Ni(II), and there was no evidence of 4:1 complexes. However, all higher generations ($n = 8$, 16, 32, 64) gave rise to predominant complexes with a 4:1 or 2:1 NH_2:Ni(II) ratio—depending on the Ni(II) and DAB-Am_n concentrations—supporting the existence of two different complexes,[26,35,36] as has been shown in previous work

(34) Cotton, F. A.; Wilkinson, G.; Murillo, C. A.; Bochmann, M. *Advanced Inorganic Chemistry*, 6th ed.; John Wiley & Sons: New York, 1999.
(35) Bosman, A. W. Ph.D. Dissertation, Technische Universiteit Eindhoven, The Netherlands, 1998.
(36) Bosman, A. W.; Schenning, A.; Janssen, R. A. J.; Meijer, E. W. *Chem. Ber.-Recl.* **1997**, *130*, 725–728.
(37) Paoletti, P.; Biagini, S.; Cannas, M. *J. Chem. Soc. D* **1969**, 513–514.

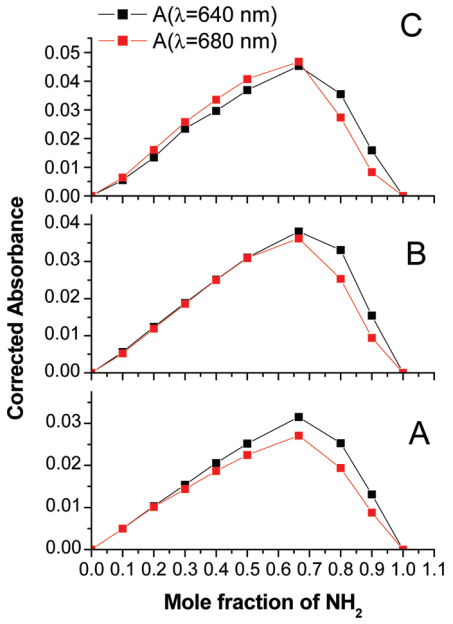

Figure 2. Job plots: absorbance at 640 and 680 nm as a function of the mole fraction of $-NH_2$ end groups for DAB-Am_4 (A), DAB-Am_{16} (B), and DAB-Am_{32} (C) with Ni(II). Total concentration of Ni(II) and dendrimer = 1×10^{-2} M. Absorbances were background corrected in all cases.

with Ni(II) and dipropyltriamine, dpt, ligand.[37−39] It was proposed that one of the complexes results from a site with six coordinating nitrogens at high DAB-Am_n−Ni(II) ratios, and the other complex comes about from a site with three coordinating nitrogens at lower DAB-Am_n−Ni(II) ratios. Based on our results here and those from previous studies,[36−39] we propose that complexation of Ni(II) by DAB-Am_n dendrimers in methanol at room temperature occurs in a site-selective way wherein dipropylenetriamine (dpt) end groups act as very strong coordinating units (Scheme 1). This outcome is similar to that we found for Cu(II) with DAB-Am_n dendrimers.[25]

DAB-Am_n−$Ni(0)_{NP}$ from DAB-Am_n−$Ni(II)_x$: Spectral Properties. Samples obtained from $NaBH_4$ reduction of DAB-Am_n−$Ni(II)_x$, (n = 4, 8, 16, 32 and 64; n/x = 4), at fixed concentration of Ni(II) were investigated by UV−visible spectroscopy. In Figure 4 are shown the optical spectra of the DAB-Am_{32}−$Ni(II)_8$ complex before and after reduction with $NaBH_4$. Upon reduction, the color of the solution changed from light green to black, indicating that DAB-Am_n-$Ni(II)_x$ is no longer present in solution. After reduction, the absorbance bands initially present at 400 and 640−680 nm are absent, and instead, a spectrum is found that has a monotonically increasing absorption with shorter wavelengths. We attribute these observations to the formation of Ni nanoparticles, because they are similar to spectroscopic results for other types of metal nanoparticles.[25,40] Indistinguishable results were observed for the other DAB-Am_n−$Ni(II)_x$ complexes.

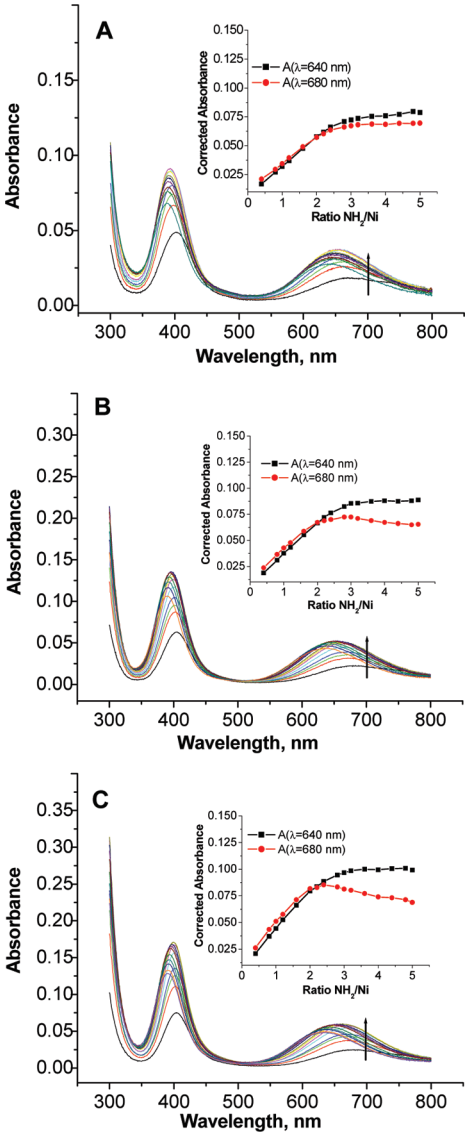

Figure 3. Titration curves for Ni(II) (A) with DAB-Am_4, (B) DAB-Am_{16}, and (C) DAB-Am_{32}. Inset: corrected absorbance at 640 and 680 nm as a function of mole ratio of $-NH_2$ end groups to Ni(II). Absorbances were corrected for dilution.

Scheme 1. Binding of Ni(II) to the Dipropyltriamine (dpt) Units of DAB Dendrimer (R = dendrimer core; DAB-Am_n)

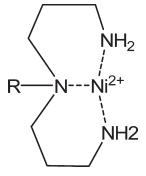

As noted in other syntheses of metallic nanoparticles,[11,41] we found that the Ni nanoparticles are not stable in aerobic environments as a result of their spontaneous surface oxidation. When DAB-Am_n−$Ni(0)_{NP}$ solutions were exposed to the laboratory ambient for times > 10 min, the color of the solutions slowly dissipated, and this is the result of the oxidation of Ni(0) to

(38) Pariya, C.; Ghosh, A.; Chaudhuri, N. R. *Thermochim. Acta* **1995**, *249*, 199–210.
(39) Vacca, A.; Arenare, D.; Paoletti, P. *Inorg. Chem.* **1966**, *5*, 1384–1389.
(40) Niu, Y.; Crooks, R. M. *Chem. Mater.* **2003**, *15*, 3463–3467.
(41) Scott, R. W. J.; Ye, H. C.; Henriquez, R. R.; Crooks, R. M. *Chem. Mater.* **2003**, *15*, 3873–3878.

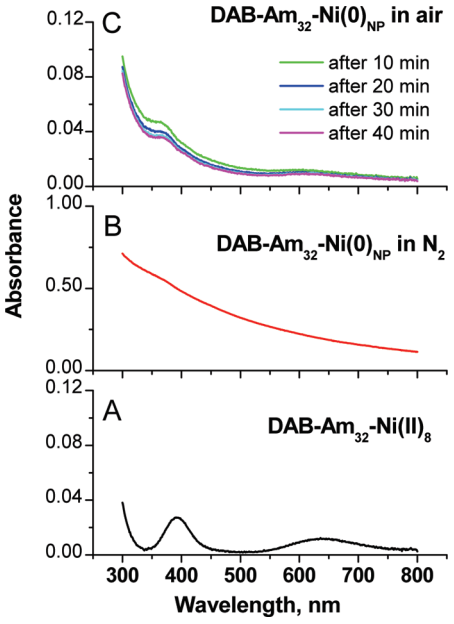

Figure 4. Absorption spectra of DAB-Am_{32}−Ni(II)$_8$ (A) before and (B) after reduction with $NaBH_4$ in methanol under nitrogen environment, and (C) subsequent exposure to laboratory ambient. [Ni(II)] = 5×10^{-4} M.

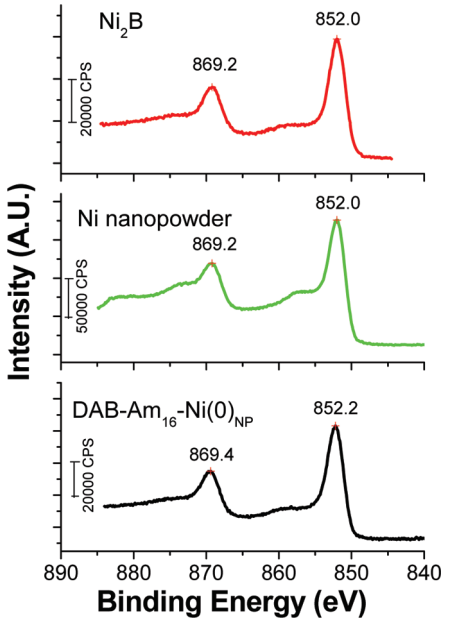

Figure 5. Ni 2p high-resolution X-ray photoelectron spectra. Bottom: Nickel nanoparticles obtained by reduction of DAB-Am_{16}−Ni(II)$_8$ ($x = n/2$; [Ni(II)] = 5×10^{-3} M). Middle: Nickel nanopowder reference ($d \leq 100$ nm). Top: Ni_2B reference.

Ni(II).[24,42] The oxidation of Ni(0) to NiO is evidenced by loss of overall absorbance and the appearance of a new and characteristic absorption peak at 370 nm (Figure 4C) that is associated with NiO.[43]

DAB-Am_n−Ni(0)$_{NP}$ from DAB-Am_n−Ni(II)$_x$ via $NaBH_4$ Reduction: Chemical Composition. XPS analyses of reduced DAB-Am_n−Ni(II)$_x$ led to more detailed information about the oxidation state of Ni and the possible presence of other elements in the nanoparticles, such as nickel borides that are often observed in borohydride-produced nanoparticles.[9] Both survey (see Figure S1 in the Supporting Information) and high-resolution spectra for the Ni 2p and B1s regions were acquired. For comparison purposes, commercially available Ni "nanopowder" (diameter ≤ 100 nm) and Ni_2B powder (30 mesh) references were evaluated.

Shown in Figure 5 is a representative high-resolution Ni 2p region spectrum of a typical borohydride-reduced DAB-Am_{16}−Ni(II) sample supported on cleaned Pt foil (see Figure S2 in the Supporting Information). The metallic nature of the Ni atoms in the reduced sample is suggested by the 852.2 eV binding energy of the Ni $2p_{3/2}$ band; however, further examination of the Ni $2p_{1/2}$ and $2p_{3/2}$ and plasmon/shakeup loss satellite transitions[44] allow for more definitive assignment of nickel valency. Confirmation of the zero-valence state of the nickel in the nanoparticles comes from the observed 17.2 eV binding energy difference between the Ni $2p_{1/2}$ and $2p_{3/2}$ transitions[45] (Figure 5) and the 6.0 eV difference in the

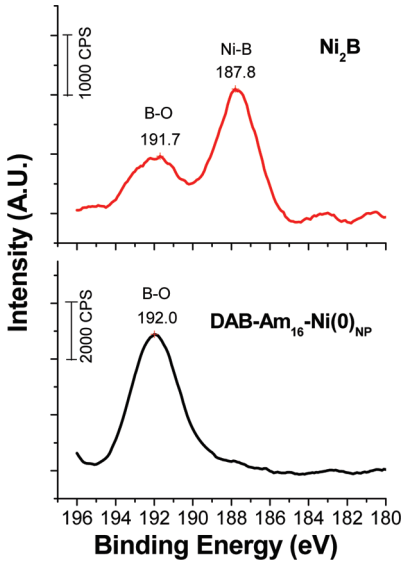

Figure 6. B 1s high-resolution X-ray photoelectron spectra. Bottom: Nickel nanoparticles obtained by borohydride reduction of DAB-Am_{16}−Ni(II)$_8$ ($x = n/2$; [Ni(II)] = 5×10^{-3} M). Top: Ni_2B reference.

$2p_{3/2}$ and plasmon/shakeup loss satellite transitions (see Figure 5 and peak-fitted spectrum in Figure S3 in the Supporting Information), with the latter being extremely sensitive to the oxidation state and environment of the nickel.[44] The difference in energy between the Ni $2p_{1/2}$ and $2p_{3/2}$ transitions in NiO has been observed to be 18.4 eV, whereas that in zerovalent nickel species is 17.4 eV, with the latter in good agreement with the 17.2 eV value observed for the DAB-Am_{16}−Ni(0)$_{NP}$.[45] Importantly, the 6.0 eV difference in the $2p_{3/2}$ and plasmon/shakeup loss satellite transitions (852.2 and 858.2 eV) found for the DAB-Am_{16}−Ni(0)$_{NP}$ is in agreement that observed for clean Ni(0) metal, 6.0 eV;[44] NiO has its $2p_{3/2}$ transition

(42) Glavee, G. N.; Klabunde, K. J.; Sorensen, C. M.; Hadjipanayis, G. C. *Langmuir* **1994**, *10*, 4726–4730.
(43) Qi, Y.; Qi, H.; Li, J.; Lu, C. *J. Cryst. Growth* **2008**, *310*, 4221–4225.
(44) Grosvenor, A. P.; Biesinger, M. C.; Smart, R. S. C.; McIntyre, N. S. *Surf. Sci.* **2006**, *600*, 1771–1779.
(45) Wagner, C. D.; Riggs, W. M.; Davis, L. E.; Moulder, J. F.; Muilenberg, G. E. *Handbook of X-ray Photoelectron Spectroscopy*; Perkin-Elmer Corporation Physical Electronics Division, 1979.

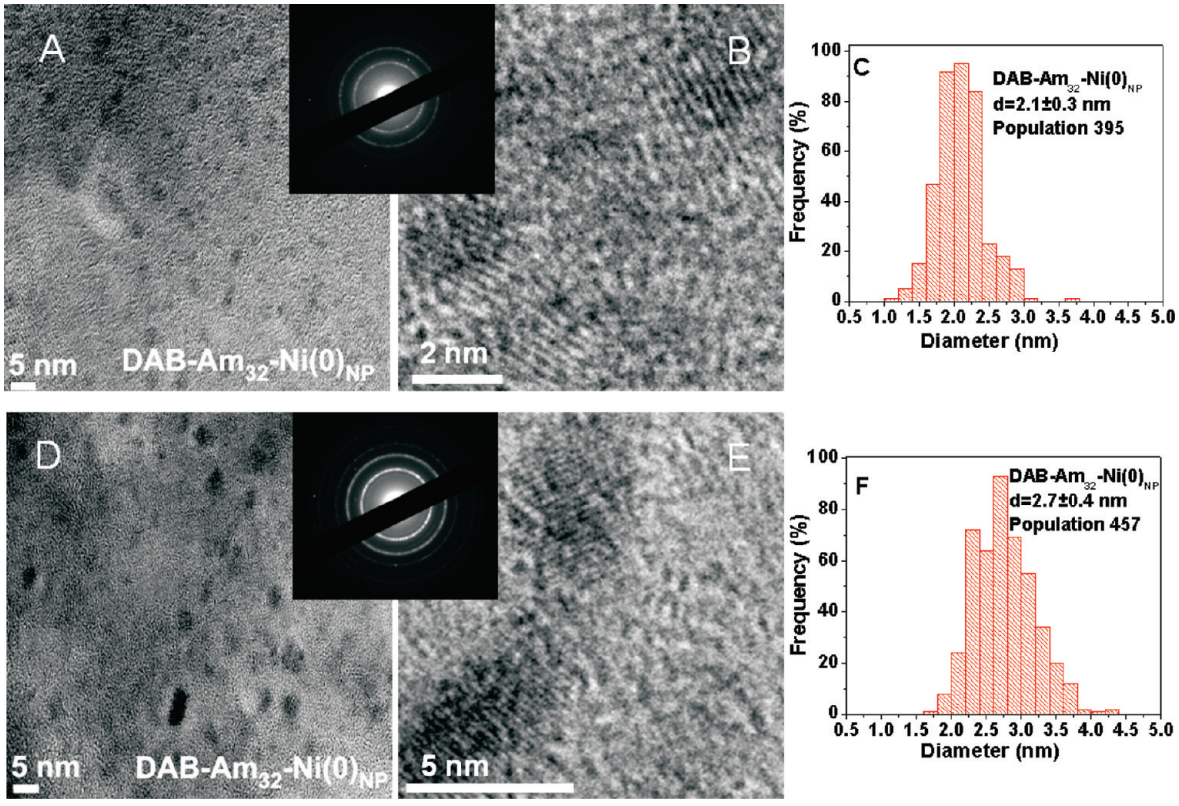

Figure 7. Representative HR-TEM images and corresponding particle size distributions of $Ni(0)_{NP}$ formed by $NaBH_4$ reduction of DAB-Am_{32}−$Ni(II)_8$, in MeOH: (A−C) for [Ni(II)] = 5×10^{-4} M and (D−F) for [Ni(II)] = 2×10^{-3} M. Insets are selected-area electron diffractograms.

centered at 854 eV and its plasmon/shakeup loss satellite located at 861 eV, whereas $Ni(OH)_2$ exhibits values of 855.4 and 861 eV.[44] Thus, we conclude that the Ni oxidation state is zero in the reduced DAB-Am_n−$Ni(II)_x$ materials.

We now turn our discussion to the well-known issue regarding the possible formation of metal borides during the borohydride reduction of metal salts, which has been observed when water or diglyme are used as solvents.[9,42] In Figure 6 are presented representative high-resolution X-ray photoelectron spectra of DAB-Am_{16}−$Ni(0)_{NP}$ and the Ni_2B reference in the B 1s region. As expected for the Ni_2B reference, a B−Ni band at 187.8 eV and that for B−O at ∼191.7 eV (in the boron oxide state) are present, and these values are in agreement with those of Ni−B alloys obtained by others.[9,46−50] The presence of oxidized boron in the Ni_2B reference is due to air oxidation, a well-known phenomenon.[9] Interestingly and importantly, the spectrum for DAB-Am_{16}−$Ni(0)_{NP}$ does not possess the characteristic B−Ni band at 187.8 eV and thus does not support the presence of any boride (B−Ni) in the Ni nanoparticles. As a result, we conclude that the borohydride reduction of DAB-Am_n−$Ni(II)_x$, under the conditions used here, results in zerovalent nickel nanoparticles free of metal boride. We postulate that this is the result of the methanol solvent employed, as it has been shown that borohydride reduction of Cu(II) in methanol results in Cu(0) particles, and not the boride.[51]

It should be noted that the spectrum for DAB-Am_{16}−$Ni(0)_{NP}$ does exhibit the characteristic B−O transition centered at 192 eV.[9] This is not surprising, as no efforts were taken to remove the other products from the synthesis because of possible oxidation and loss of the metal nanoparticles. Because of the reaction of borohydride with protic methanol to yield either methylboronate or hydrated sodium borate and hydrogen gas,[52] boron−oxygen species will always be present in the borohydride chemical reduction medium. Thus, it can be concluded that the peak at 192 eV for DAB-Am_{16}−$Ni(0)_{NP}$ is most likely associated with the presence of H_3BO_3[9,45,53] as a ∼10% impurity, but it is evidently not intimately associated with the Ni(0) nanoparticles based on results from electron microscopy studies, see below.

DAB-Am_n−$Ni(0)_{NP}$ from DAB-Am_n−$Ni(II)_x$ via $NaBH_4$ Reduction: Microscopically Determined Sizes. HR-TEM investigation of DAB-Am_n−$Ni(II)_x$ ($x = n/4$) solutions treated with a 10 mol excess of borohydride routinely lead to images such as those in A and D in Figure 7. HR-TEM images reveal the crystalline structure of the Ni(0) nanoparticles

(46) Liu, Y. C.; Huang, C. Y.; Chen, Y. W. *J. Nanopart. Res.* **2006**, *8*, 223–234.
(47) Okamoto, Y.; Nitta, Y.; Imanaka, T.; Teranishi, S. *J. Chem. Soc., Faraday Trans. 1* **1979**, *75*, 2027–2039.
(48) Li, H.; Li, H. X.; Dai, W. L.; Wang, W. J.; Fang, Z. G.; Deng, J. F. *Appl. Surf. Sci.* **1999**, *152*, 25–34.
(49) Lee, S. P.; Chen, Y. W. *Ind. Eng. Chem. Res.* **2001**, *40*, 1495–1499.
(50) Liaw, B.-J.; Chiang, S.-J.; Tsai, C.-H.; Chen, Y.-Z. *Appl. Catal., A* **2005**, *284*, 239–246.
(51) Jackelen, A.-M. L.; Jungbauer, M.; Glavee, G. N. *Langmuir* **1999**, *15*, 2322–2326.
(52) Lo, C.-t. F.; Karan, K.; Davis, B. R. *Ind. Eng. Chem. Res.* **2007**, *46*, 5478–5484.
(53) Il'inchik, E. A.; Volkov, V. V.; Mazalov, L. N. *J. Struct. Chem. (Transl. Zh. Strukt. Khim.)* **2005**, *46*, 523–534.

Table 1. Properties of Ni Nanoparticles as a Function of Dendrimer Generation upon $NaBH_4$ Reduction of Methanolic DAB-Am_n−Ni(II)$_x$ (4:1 = n/x) with Fixed [Ni(II)] = 5×10^{-4} M (BH_4^-:Ni(II) = 10:1)[a]

sample	average $Ni(0)_{NP}$ diameter ± 1 s {%} (nm)	no. of Ni atoms per $Ni(0)_{NP}$[b]	no. of DAB-Am_n−Ni(II)$_x$ required to make 1 $Ni(0)_{NP}$ [aggregate diameter (nm)][c]	Γ NH_2on $Ni(0)_{NP}$(mol cm^{-2})[d]
DAB-Am_4−$Ni(0)_{NP}$	2.7 ± 0.4 {15%}	963	963 [19]	5.58×10^{-8}
DAB-Am_8−$Ni(0)_{NP}$	2.6 ± 0.3 {12%}	890	445 [24]	5.41×10^{-8}
DAB-Am_{16}−$Ni(0)_{NP}$	2.3 ± 0.4 {17%}	611	153 [21]	4.80×10^{-8}
DAB-Am_{32}−$Ni(0)_{NP}$	2.1 ± 0.3 {14%}	428	54 [17]	4.26×10^{-8}
DAB-Am_{64}−$Ni(0)_{NP}$	1.9 ± 0.4 {21%}	325	20 [14]	3.89×10^{-8}

[a] Mean diameters (± one standard deviation {% size dispersity}) are significantly different beyond the 99.9% confidence level (as judged by application of the *t*-test to the average particle diameters of the next closest-sized particles). The number of particles used for calculating the average and standard deviation is 800, 670, 465, 395, and 355 for the 1st−5th generation dendrimer cases. [b] Calculated according to Leff et al. in *J. Phys. Chem.* **1995**, *99*, 7036−7041. [c] The aggregate diameter was computed using the method in footnote *a* and employed estimated DAB-Am_n−Ni(II)$_x$ diameters of 1.15, 1.90, 2.30, 2.72, and 3.14 nm for the n = 4−64 materials. [d] Estimated using the surface area of all nanoparticles generated by reduction and the total amount of dendrimer in solution.

Table 2. Properties of Ni Nanoparticles as a Function of Ratio of Primary Amines to Ni(II) Ions and Ni(II) Concentration in the Dendrimer Precursor[a]

NP Sample	ratio of NH_2 to Ni(II) n/x	[Ni(II)] (M)	average $Ni(0)_{NP}$ diameter ± 1 s {%} (nm)	no. of Ni atoms per $Ni(0)_{NP}$[b]	no. of DAB-Am_{32}−Ni(II) required to make 1 $Ni(0)_{NP}$ [aggregate diameter (nm)][c]	Γ NH_2 on $Ni(0)_{NP}$ (mol cm^{-2})[d]
DAB-Am_{32}−$Ni(0)_{NP}$	2:1	5×10^{-4}	2.4 ± 0.2 {8%}	702	44 [16]	2.51×10^{-8}
	4:1	5×10^{-4}	2.1 ± 0.3 {14%}	428	54 [17]	4.26×10^{-8}
		2×10^{-3}	2.7 ± 0.4 {15%}	996	125 [22]	5.65×10^{-8}
	8:1	5×10^{-4}	1.9 ± 0.4 {21%}	310	78 [20]	7.66×10^{-8}

[a] Mean diameters (± one standard deviation {% size dispersity}) are significantly different beyond the 99.9% confidence level (as judged by application of the *t*-test to the average particle diameters of the next closest-sized particles). The number of particles used for calculating the average and standard deviation is 270, 395, 457, and 500 for the 2:1, 4:1, and 8:1 ratio scenarios. The BH_4^-:Ni(II) = 10:1. [b] Calculated according to Leff et al. in *J. Phys. Chem.* **1995**, *99*, 7036−7041. [c] The aggregate diameter was computed using the method in footnote *a* and employed an estimated DAB-Am_{32}−Ni(II)$_x$ diameter of 2.72 nm. [d] Estimated using the surface area of all nanoparticles generated by reduction and the total amount of dendrimer in solution.

(Figure 7B, E) with an interplanar spacing of 0.20 nm along the (111) phase. The selected-area electron diffraction, SAED, patterns (insets in Figure 7) confirm the presence of metallic Ni, as noted by the diffraction rings from the (111), (200), (220), and (222) planes of pure Ni(0) having a face-centered-cubic (fcc) structure. No other crystalline materials can be identified in these HR-TEM and SAED images. These observations are independent of concentration of the Ni(II) in the dendrimer precursor. TEM images from control experiments of DAB-Am_n solutions treated with methanolic $NaBH_4$ did not possess any particulates. It is clear that Ni(0) nanoparticles have formed, thereby corroborating our XPS results.

We first examined the impact of dendrimer generation on $Ni(0)_{NP}$ size at fixed [Ni(II)] and $x = n/4$, as well as BH_4^-:Ni(II). HR-TEM images and particle size distributions for all dendrimer generations studied are presented in Figures S4 and S5 in the Supporting Information. The average diameters of the Ni nanoparticles as a function of dendrimer generation are compiled in Table 1, and they range between 2.7 and 1.9 nm, with notably low size dispersities. Upon statistical treatment of the $Ni(0)_{NP}$ diameter data, it was found that the differences in diameters are significant beyond the 99.9% confidence level (*t*-test). It is clear that the particle size decreases with increasing dendrimer generation. Esumi and Amis have observed a dendrimer-generation trend in Au nanoparticle size with PAMAM dendrimers as templates.[54−56]

Investigations of particle size as a function of the NH_2:Ni(II) ratio in the dendrimer precursor and nickel chloride concentration were carried out, Table 2. Upon statistical treatment of the $Ni(0)_{NP}$ diameter data, it was found that the differences in diameters are significant beyond the 99.9% confidence level (*t*-test). From the results in Table 2 and Figure S6 in the Supporting Information, it is revealed that the size of the DAB-Am_n−$Ni(0)_{NP}$ is affected by variation of the NH_2:Ni(II) ratio at fixed Ni(II) concentration. A significant decrease in $Ni(0)_{NP}$ size (~21%, or 2.26-fold decrease in number of Ni atoms) was obtained by increasing the NH_2:Ni(II) ratio in the dendrimer precursor from 2 to 8 at fixed Ni(II) concentration, (Table 2 and Figure S6 in the Supporting Information). In addition, there is a roughly 30% increase in particle size with an increase of the [Ni(II)] from 5×10^{-4} to 2×10^{-3} M (Figure 7).

At this point, we turn to a discussion of $Ni(0)_{NP}$ formation from the DAB-Am_n−Ni(II)$_x$ materials upon addition of BH_4^-. From the data in Tables 1 and 2, it is clear that the size dispersity of the $Ni(0)_{NP}$ is relatively invariant with respect to the various conditions for their preparation. Furthermore, the size dispersity is very small in all cases (8−21%). These results—according to nucleation theory[57]—point to the

(54) Esumi, K.; Suzuki, A.; Yamahira, A.; Torigoe, K. *Langmuir* **2000**, *16*, 2604–2608.
(55) Esumi, K.; Suzuki, A.; Aihara, N.; Usui, K.; Torigoe, K. *Langmuir* **1998**, *14*, 3157–3159.
(56) Gröhn, F.; Bauer, B. J.; Akpalu, Y. A.; Jackson, C. L.; Amis, E. J. *Macromolecules* **2000**, *33*, 6042–6050.
(57) Finney, E. E.; Finke, R. G. *J. Colloid Interface Sci.* **2008**, *317*, 351–374.

Scheme 2. Proposed Path for Formation of DAB-Am$_n$−Ni(0)$_{NP}$

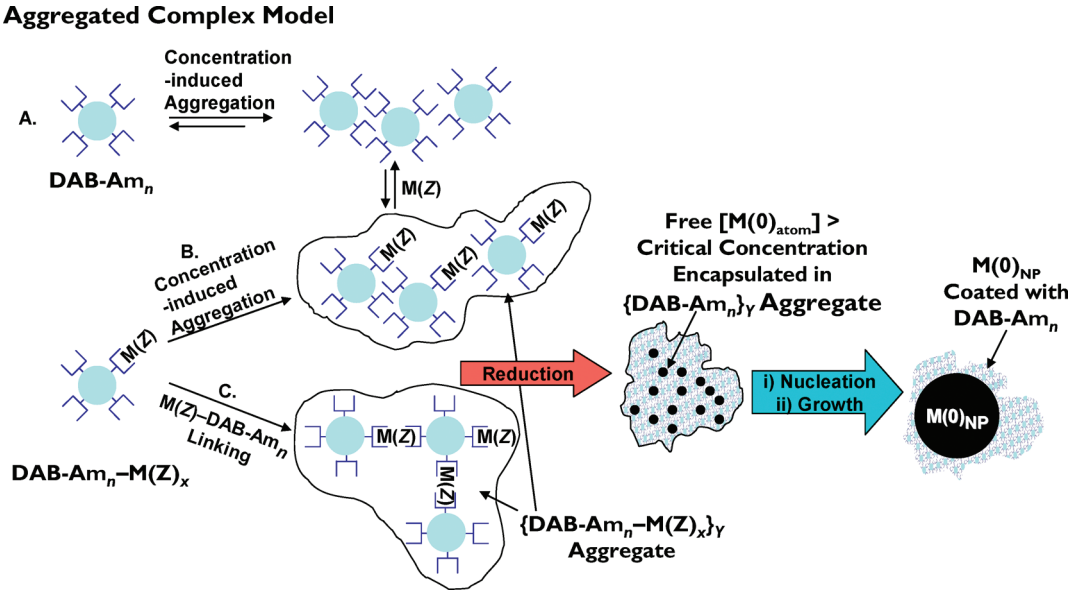

separation of the nucleation event from that of the particle growth event, either temporally or spatially. That is to say, the variation in size of the nanoparticles is small because the production of critical nuclei is very near completion before the onset of nuclei enlargement by addition of Ni(0) atoms. Typically, this is achieved by either kinetic (temporal) or steric (spatial) constraints, wherein either reducing agent is added extremely quickly to the metal ion solution or the metal ions are sequestered in a fixed volume through use of template molecules/assemblies during the reduction process.[57] Importantly, under the conditions used here, the BH_4^- reducing agent was added at a relatively slow rate (0.5 mL in 30 s); thus the low size dispersities observed here are attributed to a scaffold effect imparted by the DAB-Am$_n$ environment. A strong interaction of the dpt groups of DAB-Am$_n$ with Ni(II)—$K = 2.45 \times 10^7$ for methyl-dpt of Scheme 1 ($R = CH_3-$)[58]—and the resulting Ni(0) surface will result in a small Ni(0)$_{NP}$ size dispersity and Ni(0)$_{NP}$ size, as noted in a study of Pt and Pd nanoparticles produced from a select group of DAB-Am$_n$ ($n = 8$, 16, 32) at extremely high primary amine:metal ion ratios ($200 \leq n/x \leq 800$).[28]

We observe very small Ni(0)$_{NP}$ sizes that are highly dependent on dendrimer generation (Table 1) and NH_2:Ni(II) values of $2 \leq n/x \leq 8$ (Table 2). Ni(0)$_{NP}$ size is inversely proportional to dendrimer generation and NH_2:Ni(II) ratio (n/x). Because of the sizes of the DAB-Am$_n$ in solution, the Ni(0)$_{NP}$ produced here cannot reside completely inside the dendrimers, and it is concluded that the nanoparticles are coated with the DAB-Am$_n$ (interdendrimer), yielding a nanocomposite material, similar to what we proposed in an initial study with Cu(II)-PPI complexes and that proposed by Gröhn et alia for PAMAM-Au(III) materials.[25,56] For example, in the case of the fifth-generation dendrimer in Table 1, the resulting Ni nanoparticle has a diameter of 1.9 nm that is only slightly smaller than that of DAB-Am$_{64}$ (~2.5 nm); these observations are in accord with those from our work with DAB-Am$_n$−Cu(0)$_{NP}$ nanocomposites.[25] In addition, it is clear that the number of Ni atoms contained in a single Ni(0)$_{NP}$ is more than that available in an individual precursor, DAB-Am$_n$−Ni(II)$_x$, which upon initial examination would seem to indicate that the growth process of the Ni(0) nuclei is not well separated from nuclei formation; however, this cannot be the case as the size dispersity of the Ni(0)$_{NP}$ is very low. Finally, the inverse relationship between Ni(0)$_{NP}$ size and n/x (NH_2:Ni(II) ratio, Table 2) would at first glance lead to the conclusion that the developing nanoparticle is stabilized by the presence of more amine groups on its surface (see last column in Table 2), but this argument does not hold for the generation-dependent effects observed in Table 1. Similar attempts on our part to describe the mechanism of DAB-Am$_n$−Cu(0)$_{NP}$ formation were met with similar frustration, but in that study we did not have detailed data regarding the effects of NH_2:metal ion ratio on nanoparticle size.[25]

We propose that the observed inverse relationship between Ni(0)$_{NP}$ size and both dendrimer generation and NH_2:Ni(II) ratio (n/x), and the larger-than-expected Ni(0)$_{NP}$ size, are due to the presence of DAB-Am$_n$−Ni(II)$_x$ complex aggregates, whose size is dependent on the concentration and generation of DAB-Am$_n$−Ni(II)$_x$ in the methanol solutions. As outlined in Scheme 2, we posit that upon {DAB-Am$_n$−Ni(II)$_x$}$_Y$ exposure to reducing agent, nanoparticles of a dimension corresponding to the total number of Ni atoms initially in the aggregate (n^*Y/x) are formed, and the resulting Ni(0)$_{NP}$ are protected from further growth by their presence within the dendrimer aggregate. The aggregates of Ni(II)-dendrimer complexes form either as a result of the Ni(II) coordinating to preexisting aggregates of the DAB-Am$_n$ (path A in Scheme 2), or they form by aggregation of the DAB-Am$_n$−Ni(II)$_x$ complexes (paths B and C in Scheme 2). Upon reduction of the Ni(II)-complex aggregates, the concentration of the

(58) Goldberg, D. E.; Fernelius, W. C. *J. Phys. Chem.* **1959**, *63*, 1328–1330.

$Ni(0)_{atom}$ species is above the supersaturation value ("critical value"), and nucleation occurs in the $\{DAB\text{-}Am_n\}_Y$ aggregate to yield $DAB\text{-}Am_n{-}Ni(0)_{NP}$. This model is in accord with the larger-than-expected sizes of the $Ni(0)_{NP}$ found here and those in our previous study of $Cu(0)_{NP}$,[25] as well as the small size dispersity of the nanoparticles. In preliminary dynamic light scattering studies of $DAB\text{-}Am_n$ in methanol with added Cu(II), we find evidence for aggregation of $DAB\text{-}Am_n{-}Cu(II)_x$, and the aggregation behavior is a function of both the concentration of the dendrimer-metal ion complex and the NH_2:Cu(II) ratio (n/x).[59] At concentrations above roughly 1×10^{-3} M of dendrimer NH_2 groups, aggregates ~35 nm in diameter were observed for $DAB\text{-}Am_{16}{-}Cu(II)_x$ and $DAB\text{-}Am_{32}{-}Cu(II)_x$; this value is most likely an overestimate of aggregate size, because of the interfering effects of light absorption by the sample.[60] We conclude that aggregate formation would also occur for Ni(II), based on its similar chemical properties in comparison to Cu(II).[5] At this time, we cannot discern between paths B and C in Scheme 2, but it is clear that aggregation of the $DAB\text{-}Am_{32}{-}Ni(II)_x$ would lead to the results noted in Tables 1 and 2.

Conclusions

Ni(II) has been shown to form well-defined, stoichiometric complexes with $DAB\text{-}Am_n$ dendrimers in methanol. Using UV−vis spectroscopy and the method of continuous variation, as well as titrations, it was determined that the predominant complex between Ni(II) and all $DAB\text{-}Am_n$ dendrimer generations studied exhibits a 2:1 ratio of NH_2 end groups to Ni(II). Crystalline Ni(0) nanoclusters possessing a fcc structure, with diameters ranging from 1.9 to 2.7 nm, have been prepared by methanolic $NaBH_4$ reduction of Ni(II) coordinated to various generations of $DAB\text{-}Am_n$ dendrimers (1, 2, 3, 4, and 5) under a variety of conditions. From XPS characterization studies, it was found that the Ni nanoparticles prepared by the dendrimer−ligand-based method are in the metallic state without any Ni−B alloy present, and they possess an impurity of H_3BO_3 that forms during decomposition of $NaBH_4$ in methanol solution. The size of the Ni(0) nanoparticles can be precisely controlled (in order of impact) via dendrimer generation or the ratio of primary amines to Ni(II) ions in the dendrimer precursor. We would like to expand the variety of metal ions that can be complexed by $DAB\text{-}Am_n$ dendrimers using the dendrimer−ligand-based method in order to create new hybrid materials, such as bimetallic nanoparticles supported on silica surfaces for environmental catalysis applications.

Acknowledgment. The authors thank the National Science Foundation for financial support of this work and LSU Graduate School. In addition, we thank Dr. Dongmei Cao for assistance with obtaining TEM images.

Supporting Information Available: XPS data, HR-TEM images, and particle size distribution of nickel nanoparticles (PDF). This material is available free of charge via the Internet at http://pubs.acs.org

(59) Bantchev, G. B.; McCarley, R. L. **2010**, unpublished results.
(60) Schaertl, W.; Roos, C. *Phys. Rev. E* **1999**, *60*, 2020–2028.